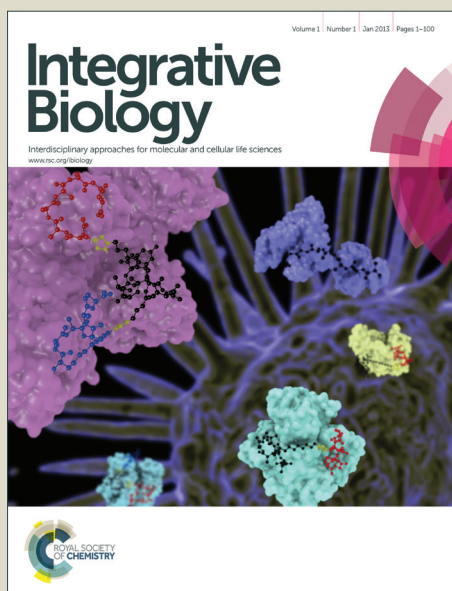


Integrative Biology

Accepted Manuscript



This is an *Accepted Manuscript*, which has been through the Royal Society of Chemistry peer review process and has been accepted for publication.

Accepted Manuscripts are published online shortly after acceptance, before technical editing, formatting and proof reading. Using this free service, authors can make their results available to the community, in citable form, before we publish the edited article. We will replace this *Accepted Manuscript* with the edited and formatted *Advance Article* as soon as it is available.

You can find more information about *Accepted Manuscripts* in the [Information for Authors](#).

Please note that technical editing may introduce minor changes to the text and/or graphics, which may alter content. The journal's standard [Terms & Conditions](#) and the [Ethical guidelines](#) still apply. In no event shall the Royal Society of Chemistry be held responsible for any errors or omissions in this *Accepted Manuscript* or any consequences arising from the use of any information it contains.

Insight statement

Genome function is related to how DNA is differentially packed into chromatin inside the eukaryotic cell nucleus. DNA that is tightly packed has limited function whereas opened DNA is highly accessible for genome regulation. In this study, we show that cellular mechanical signals via the actin cytoskeleton could dictate DNA packing, by altering the dynamics of nuclear proteins that are involved in both mechanosensing and DNA packing mechanisms.

Title

Actin cytoskeleton differentially alters the dynamics of lamin A, HP1 α and H2B core histone proteins to remodel chromatin condensation state in living cells

Author Affiliations

Kee Chua Toh^{1,*}, Nisha M. Ramdas^{2,*}, G.V. Shivashankar^{1,3,4,†}

¹Mechanobiology Institute, National University of Singapore, Singapore 117411

²National Centre for Biological Sciences, Tata Institute of Fundamental Research, Bangalore 560065, India

³Department of Biological Sciences, National University of Singapore, Singapore 117543

⁴Centre for Bio-Imaging Sciences, Department of Biological Sciences, National University of Singapore, Singapore 117543

*Authors contributed equally to the work

†Corresponding author

Corresponding Author

G.V. Shivashankar, Mechanobiology Institute, National University of Singapore, T-Lab #05-01, 5A Engineering Drive 1, Singapore 117411. Email: shiva.gvs@gmail.com

Abstract

Cells in physical microenvironments regulate their functioning and geometry in response to mechanical stimuli. Recent studies have demonstrated the influence of the integrated actin cytoskeleton on nuclear integrity and chromatin organization. However, the mechanisms underlying the mechanotransduction of their physical coupling to nuclear protein dynamics is not well understood. In this study, we take advantage of micropatterned geometric substrates in NIH3T3 mouse fibroblasts, to probe the functional influence of actin organization on nuclear lamina and chromatin assembly. Fluorescence correlation spectroscopy studies demonstrate that stabilization of perinuclear actin strengthens the transient interactions of lamin A with the chromatin. Correspondingly, fluorescence recovery after photobleaching studies reveals an enhanced mobility of these nuclear lamina proteins when actin organization is perturbed. Combining these fluorescence dynamics assays, we also demonstrate an actin-driven differential modulation of core histone H2B and heterochromatin HP1 α protein dynamics with chromatin. These altered dynamics are reflected structurally by concomitant changes in the architecture of the heterochromatin foci as seen by immunofluorescence assays. Taken together, our study provides a demonstration of the differential mechanical control of perinuclear actin on the dynamics of the nuclear lamina, euchromatin and heterochromatin regimes of the nucleus, and suggests an actin-mediated route to spatially and structurally tune chromatin organization and dynamics.

Introduction

In lineage specific cells there is a fine balance between cytoskeleton organization and chromatin assembly to facilitate functional genome organization¹⁻³. Evidence has shown that the differential condensation of chromatin into distinct spatiotemporal architectural domains⁴⁻⁶ are established through proteins whose dynamics are thought to impinge on gene expression⁷⁻⁹. Studies have shown that there are direct links from the cytoskeleton to the nuclear membrane, and from the nuclear membrane to chromatin via the lamin network¹⁰⁻¹³. Importantly, there exists a tight physical coupling between actin and lamin architectural assemblies¹⁴ which is reflected functionally. Alteration to lamin A/C organization influences actin dynamics resulting in altered nuclear mechanotransduction and cellular functioning¹⁵⁻¹⁸. Concomitantly, perturbation of the actin architecture has been found to alter lamin A/C mechanical integrity as well as nuclear organization^{19,20}. Substrate rigidity or geometry has a profound impact on cytoskeleton remodeling and subsequent changes in gene expression as revealed by cell analysis^{21,22}. Emerging studies have also shed light on the influence of actin and microtubule assemblies on cell migration, as well as chromatin organization and its condensation states²³⁻²⁶. Our recent studies have revealed molecular components that link the cytoskeleton mediated coupling to nuclear morphology and chromatin dynamics²⁰. However, the mechanisms underlying the active physical cytoskeleton-to-nuclear mechanotransduction are unclear. In particular, the functional coupling of lamin A/C, HP1 α and H2B proteins to actin architectural networks has not been understood.

The spatiotemporal organization of chromatin within the cell nucleus underlies the cellular control of gene expression^{6, 27}. The differential condensation of the chromatin into transcriptionally active euchromatin and transcriptionally less active heterochromatin is mediated through the hierarchical organization of core histone and linker proteins²⁸, with epigenetic modification on histone tails serving as a regulator of the cellular genetic code²⁹.

The heterochromatin protein HP1 α is a nonhistone chromosome-binding protein that plays an important role in stabilizing the heterochromatin domains through dynamic binding and dissociation. HP1 α consists of an N-terminal chromodomain (CD) and a C-terminal chromo shadow domain (CSD). For gene silencing, the CD domain of the proteins interacts with the H3 histone tails that carry the K9me2/3 modification^{30,31}. The CSD, however could bind to various HP1 binding proteins that are involved in gene transcription. This organization of interphase chromosomes into specific compartments and territories is important for chromatin function and gene transcription regulation^{6,27,32-34}.

In this study, we employ micropatterned substrates to alter the cellular geometry of NIH3T3 fibroblasts and quantitatively analyse the spatiotemporal dynamics of adaptor proteins that couple the nuclear membrane to chromatin. Our work demonstrates the differential influence of perinuclear actin on nuclear protein dynamics and provides important insights into dynamic reorganization of protein assemblies central to nuclear mechanotransduction.

Results & Discussions

Cell geometric constraints demonstrate structural modulation of nuclear lamin A/C protein

In order to assess the influence of the actin cytoskeleton on nuclear lamina integrity, the cells were subjected to geometric constraints and subsequent alterations in actin organization were observed. Illustrated in Figure 1A are representative images of phalloidin-stained actin architectural influence on nuclear organization. The lamin A/C stained nuclear lamina and Hoechst stained DNA in NIH3T3 cells grown randomly (cells-Unpatterned)) on fibronectin-coated surfaces, are shown in contrast to geometry constrained fibronectin patterned cells grown on 1800 μm^2 rectangular-patterns (cells-(Rectangle)) and 500 μm^2 circular-patterns (cells-(Circle)) (Fig S1A). Basal to apical sections through the cell depict nuclei flattened by

perinuclear actin stress fibre organization in cells-(Unpatterned), with cellular architecture in cell-(Rectangle) showing similar flattened architecture though constrained by geometry. In contrast, cells-(Circle) exhibit perturbation to apical actin organization and consequently have elongated nuclei with smaller projected area (Fig S1B). Additionally, due to loss of actin stresses, they exhibit large variation in nuclear shape along the height of the nucleus (Fig S1C).

To assess changes in the spatial organization of nuclear lamin A/C, we measured the protein expression levels using immunofluorescence staining. Using confocal images of z-sections of nuclei in cells in different geometries, we found a marked reduction in global lamin A/C intensity levels in cells-(Circle) (Fig 1B) in comparison to the cells-(Unpatterned) and cells-(Rectangle). This was consistent with earlier reports of lamin A/C scaling with nuclear projected area³⁵. Additionally, an increased heterogeneity in lamin A/C organization is reflected by enhanced intensity variation across the z-projected lamin A/C images (Fig S1D). The observed alteration to nuclear lamin organization with geometry-mediated changes in actin demonstrates the role of perinuclear actin on the nuclear lamina, in agreement with earlier reports of actin influence on nuclear morphology^{19,21}.

FCS experiments reveal two distinct time components for Lamin A, HP1 α and H2B mobility within the nucleus of living cells

To understand how the actin organization influences nuclear proteins and subsequently leads to changes in chromatin organization, we examined its influence on the dynamics of three types of nuclear proteins: nuclear lamina component lamin A, heterochromatin protein HP1 α , and core histone H2B proteins. We employed fluorescence correlation spectroscopy (FCS) as a probe of the diffusion timescale of these nuclear proteins, each transiently tagged with eGFP. The influence of cell geometry on diffusion characteristics was examined with the

autocorrelations curves for the FCS data fitted using a two-component (i.e. fast and slow component) 3D diffusion model (SI Materials and Methods, Fig S2).

Figure 2A shows the distribution profile of the fast component for each of the nuclear proteins in cells-(Unpatterned), obtained from the accumulation of all FCS experiments in this study. The lamin A FCS data shows the fast component has a log normal distribution which peaks at 755 μs and with a mean correlated time of $1064 \pm 520 \mu\text{s}$ (Fig 2A). We attribute this fast component to be the diffusion of proteins in the nucleus hereafter. This leads to a diffusion constant of $12.2 \mu\text{m}^2\text{s}^{-1}$ for lamin A as derived from the FCS data. The mean diffusion time for HP1 α fast component is $1109 \pm 384 \mu\text{s}$, with a log normal diffusion time distribution similar to lamin A, and this HP1 α distribution peaks at $\sim 905 \mu\text{s}$. The corresponding diffusion constant for this fast component in nucleus is $D_{\text{HP1}\alpha\text{complex}} = 11.7 \mu\text{m}^2\text{s}^{-1}$. For histone H2B proteins, the diffusion time obtained from the FCS data is found to be 633 μs with the corresponding $D_{\text{H2B}} = 20.6 \mu\text{m}^2\text{s}^{-1}$.

In contrast to the fast component, the slow component contains the information of the active association and dissociation of the tagged protein in a supercomplex or a molecular network during the reactive period of a molecular complex transiently bound to a molecular network^{36, 37}. Those inactive tagged protein associated in a molecular network, longer than the FCS data collection time, would not be contributed to the FCS signal. We henceforth refer to this slow component as the interaction time, and un-patterned cells without drug treatment as control. However we must note that proteins tightly bound to the chromatin network will also show slow fluctuations probably in the 100 ms range due to motion of the chromatin fibers to which the proteins are bound. From the lamin A FCS data, the effective diffusion constant derived from the interaction time is $1.0 \mu\text{m}^2\text{s}^{-1}$, which is considerably faster than $0.38 \mu\text{m}^2\text{s}^{-1}$ as reported in the HeLa cell line³⁸. The mean interaction time for HP1 α and H2B obtained from the FCS data are 24.6 and 26.1 ms, respectively (Fig 2B, Summary in Table S2), with

derived effective diffusion constants of 0.53 and $0.50 \mu\text{m}^2\text{s}^{-1}$, respectively. The corresponding fraction of the interacting component is found to be 54 ± 9 % for lamin A, 51 ± 8 % for HP1 α , and 26 ± 12 % for H2B (Table S3). These interacting component fractions would give us an idea how active the proteins are at the molecular level, for example, our study shows lamin A and HP1 α are more dynamic and active when compared to H2B.

Cell-geometric constraints differentially alter Lamin A, HP1 α and H2B dynamics

Using cells grown on fibronectin-coated micro-patterns we further assessed the influence of cellular geometry on the dynamics of lamin A, HP1 α and H2B proteins. Figures 2C-E illustrates the modulation in FCS two-component interaction timescales for each of the proteins. The FCS data for lamin A in cells-(Rectangle) has a mean interaction time of 19.3 ± 7.6 ms as shown in Fig 2C, which is longer than in un-patterned cells ($P < 0.001$). For cells-(Circle), the mean interaction time is 18.6 ± 7.5 ms ($P < 0.001$ when compared to control), indicating a strengthening of transient interaction of lamin A in cells-(Circle) as well. This increase in transient interaction time is also observed for HP1 α located at the nuclear periphery. The measured mean interaction time for HP1 α in cell-(Rectangle) is 35.3 ± 18.0 ms as shown in Fig. 2D, an increase from the ~ 25 ms time in un-patterned ($P < 0.001$). For HP1 α in cells-(Circle), the mean interaction time is 28.4 ± 9.7 ms (not significantly different from the HP1 α in the un-patterned cells), indicating a decrease in the interaction of HP1 α when compared to cells-(Rectangle). Strikingly, the mean interaction time for histone H2B found in cell-(Rectangle) is 17.2 ± 7.7 ms (Fig 2E, $P < 0.001$ when compared to un-patterned cells). The histogram for the interaction times of eGFP-tagged H2B in cells-(Circle) was found to have higher heterogeneity with a mean interaction time of 31.4 ± 19.9 ms. This heterogeneity in transient interaction time strongly suggested an increase in chromatin activity in the nucleus.

Actin perturbation using drugs leads to alteration of lamin A, HP1 α and H2B interaction timescales that mirrors the alterations observed from geometric constraints

We further assessed whether perturbation of actin architecture through modulation of the actin polymerization state using pharmacological reagents could also result in alteration to nuclear protein dynamics. Figure 3A shows representative basal and apical cellular images depicting enhanced actin polymerization using the actin stabilizing drug jasplakinolide (Jas)³⁹, and conversely, perturbed actin organization using the actin depolymerization drug latrunculin A (LatA)⁴⁰.

Examination of lamin A, HP1 α and H2B dynamics in the pharmacologically perturbed cells (Fig 3B-D) showed a differential modulation of interaction timescales, mirroring that seen by geometric constraints. Lamin A in the Jas treated cells (cells-(Jas)) (Fig 3B) showed an enhanced mean interaction time of 25.4 ± 9.6 ms ($P < 0.001$), in contrast to Lat A treated cells (cells-(LatA) which revealed a minimal change in the transient binding of 14.3 ± 5.9 ms ($P < 0.001$ vs. cells-(Jas), $P < 0.05$ vs. un-patterned cells)). Correspondingly, the assessment of HP1 α (Fig 3C) in cells-(Jas) also revealed a marked increase in interaction time to 33.4 ± 15.9 ms ($P < 0.001$), with a similar minimal change in transient binding of 26.9 ± 9.4 ms in cells-(LatA) (not significantly different from the un-patterned cells). The investigation of H2B (Fig 3D), showed that the overall mean interaction time instead decreased significantly to 16.6 ± 7.6 ms ($P < 0.001$) in cells-(Jas) indicating a marked change in histone activity. However, though the mean interaction time of H2B in cells-(LatA) was found to be similar to cells-(Unpatterned), further investigation revealed a broader distribution of interaction timescales (Fig 3D, $P < 0.05$ for test for variance). This enhanced heterogeneity in the interaction timescales of protein dynamics mirrored the heterogeneity seen due to circular geometric constraints (Fig 2E). Additionally, we found that cells-(Unpatterned) that were subjected to serum starvation demonstrated enhanced HP1 α interaction timescales, and

concomitantly lowered H2B interaction timescales, consistent with the influence of actin stabilization on nuclear protein dynamics in our cells-(Rectangle)/cells-(Jas) assays (Fig S3) and this indicated a chromatin compaction state^{41, 42}.

Mobility of nuclear proteins are differentially modulated by cellular geometric constraints

To further probe the dynamics of these nuclear proteins, we used fluorescence recovery after photobleaching (FRAP), using recovery kinetics as a reflection of chromatin dynamics. Illustrated in Fig 4A are time-lapse images of lamin A recovery dynamics altered by cellular geometry. The lamin A bleach recovery of 5 – 7 % in cells-(Rectangle) (Fig 4B) indicates that the nuclear envelope protein is largely immobile in the flattened geometry similar to cells-(Unpatterned), and as evidenced by earlier studies⁴³. The FRAP analysis in cells-(Jas) (Fig 4C) with altered polymerization state also revealed similar kinetics. In contrast, we observed a modulation to protein dynamics in cells-(Circle) demonstrated by 16-18% increase in recovery of lamin A proteins. Additionally, the investigation of protein dynamics in actin perturbed cells-(LatA) revealed similar recovery dynamics reflective of higher protein mobility. Our results therefore revealed enhanced mobility of lamin A when F-actin was perturbed either due to geometry or polymerization state, indicating that actin architecture strongly affects lamin A mobility. This correlation between lamin A deficiency and chromatin organization is similar to earlier reports of enhanced mobility in lamin altered cells⁴⁴ and reports showing that histone modifications and lamina regulate chromatin dynamics^{45, 46}.

For HP1 α and H2B FRAP studies, we distinguished between the heterochromatin foci and euchromatin domains based on high or low contrast chromatin regions using either HP1 α or H2B protein spatial organizations in the transfected cell, respectively. We restricted our probe

of HP1 α to only heterochromatin foci domains, and our probe of H2B to only euchromatin domains. Earlier reports have shown H2B to be distributed in cell nuclei similar to that of DNA⁴⁷. Our FRAP study of the core histone euchromatin dynamics (Fig 4H-I) on cells-(Unpatterned) revealed a small mobile population (~7%), with a large slow mobile/immobile population consistent with earlier reports^{47, 48}. In contrast, our investigation showed that perturbation to actin organization resulted in enhanced histone dynamics in comparison to the dynamics in flattened cell nuclei (Fig 4G). The analysis of fluorescence recoveries revealed a faster recovery and higher mobile fraction of the H2B protein (~11%) in the nuclei of cells altered both due to geometry (cells-(Circle)) (Fig 4H) as well as pharmacological reagents (cells-(LatA)) (Fig 4I). These results thus revealed the functional relevance of actin organization on euchromatin dynamics, consistent with the shorter transient interaction timescales as revealed by the FCS distribution profiles (Fig 2E, Fig 3D). However, the study of HP1 α heterochromatin foci dynamics revealed a differentiation in mobility dynamics (Fig 4D-F). HP1 α proteins have been shown to dynamically associate with chromatin, with faster dynamics in euchromatin regions in comparison to heterochromatin regions³⁰. Illustrated in Fig 4D are representative time-lapse images of HP1 α recovery dynamics in cells constrained by substrate geometry. HP1 α proteins are highly mobile (~75%) with a small immobile population^{30, 49, 50} on cells-(Unpatterned) or cells-(Rectangle). However, we found a lowered fraction (~67%) of mobile HP1 α proteins in the heterochromatin foci of nuclei with actin organization lost either due to patterns (cells-(Circle)) or due to pharmacological agents (cells-(LatA)) (Fig 4E-F). Our investigation of these spatially organized chromatin domains therefore revealed that altered actin organization resulted in constrained mobility at heterochromatin domains in contrast to enhanced mobility at euchromatin domains. In summary, our FRAP probe demonstrated differential actin-mediated influence at the nuclear lamina, and the two differentially compacted chromatin regimes.

Chromatin spatial organization responds to geometrical constraints without significantly changing the protein level of HP1 α and H3K9me3

To further assess the relevance of these changes in protein dynamics, we employed immunofluorescence (IF) assays to probe whether these dynamic changes were reflected by functional changes in the organization of nuclear proteins. Figure 5A shows confocal images of Hoechst stained DNA, HP1 α , and the corresponding histone H3 trimethylated at lysine 9 (the H3K9me3 epigenetic marker) in the cell nuclei grown on different geometric patterns. H3K9me3 is a known indicator of chromatin compaction state due to its involvement in heterochromatin formation and transcription repression^{51, 52}. Both HP1 α and H3K9me3 immunofluorescence images mark similar spatially compacted chromatin domains as labelled by Hoechst stained DNA, and reflected by the merge of the images. A quantitative assessment of the immunofluorescence based on HP1 α protein levels and H3K9me3, however, revealed no significant change in the global levels of the proteins (Fig 5B–C). Thus, neither the HP1 α nor the H3K9 trimethylation levels provided an explanation for the changes in chromatin dynamics. Further analysis of the confocal images demonstrated differences in chromatin spatial organization as reflected by changes in the heterochromatin foci organization. A quantitative assessment of these changes was described by the analysis of heterochromatin foci surface area in Figure 5D, indicative of larger heterochromatin foci in nuclei in cells-(Circle). In addition, we found evidence of enhanced condensation in heterochromatin foci reflected by higher heterochromatin/euchromatin intensity ratio (Fig S4A).

Our results suggest that, while some regions (heterochromatin) of the chromatin are being more condensed, other regions in contrast are being less condensed by cell geometric constraints. Consistent with this, H2B FRAP studies demonstrate an increased recovery of histones in cells-(Circles), when compared to cells-(Unpatterned) and cells-(Rectangular).

Our results point to important insights towards the mechanical control of differential chromatin compaction states, although the underlying molecular mechanisms are still unclear. These changes are demonstrative of the functional role of actin organization on chromatin spatial organization, and could serve as a structural means to support the recent reports of the role of heterochromatin protein influence on gene expression.

In summary we show that the polymerization state of actin, modulated via cell geometry, regulates the dynamics of chromatin assembly. The strengthening of lamin A protein interaction by F-actin is an important factor to promote dynamic equilibrium between heterochromatin and euchromatin assembly. Taken together, our results suggest that nuclear mechanotransduction processes could serve as integrated forward and backward feedback systems, mechanically coupling actin and chromatin assembly via the nuclear lamins to tune the epigenetic modifications by various regulatory proteins.

Acknowledgements

We thank Prasuna Rao for the qPCR experiments and Andrew Wong Ming-Shang for critically reading the manuscript. This work is supported by the Mechanobiology Institute, and Singapore Ministry of Education (MOE) Academic Research Funding (AcRF) Tier 3.

Key words

actin, chromatin remodeling, heterochromatin, histones, nuclear lamin, mechanical sensing, mechano-transduction, fluorescence correlated spectroscopy (FCS), fluorescence recovery after photobleaching (FRAP)

Materials and Methods

Cell culture and micro-patterning

NIH 3T3 (ATCC®) fibroblast cells were cultured in growth medium containing low glucose Dulbecco's modified Eagle's medium (DMEM) (Life Technologies) supplemented with 10% Fetal Bovine Serum (FBS) (GIBCO, Life Technologies) and 1% Penicillin-Streptomycin (Life Technologies) at 37°C with 5% CO₂. Cells were incubated on fibronectin coated micro-patterns for 3 hr before imaging or fixation. For alteration of actin filament organization via drugs, cells seeded on micropatterns were treated with Latrunculin A (Sigma-Aldrich®) or Jasplakinolide (AG Scientific, Inc.) at a concentration of 60-100 nM (with less than 0.1 µl of DMSO in 1 ml of final growth medium). The micro-patterned polydimethylsiloxane (PDMS) stamps were made from PDMS elastomer (Sylgard® 184; Dow Corning) as described earlier²³. For FCS experiment, cells were seeded onto pretreated glass surface dishes (IWAKI, Asahi Glass Co., Ltd. Japan): spin coated (Laurell Technologies Corporation, WS-400BZ-6NPP\LITE, 6000 rpm for 2 minutes) with a layer of 5 µm PDMS (with 1:5 ratio of curing agent in the mixing) and cured at 80°C for 3 hr, prior to surface treatment with high intensity UV radiation (UV/Ozone Procleaner™ Plus, Bioforce Nanoscience) for 2 min. For immunofluorescence and FRAP experiments, the plastic bottom dish (ibidi®) was used without any prior treatment. The FCS and FRAP experiments were performed on eGFP-tagged to nuclear lamin A (purchased from addgene plasmid #17662, originally from Tom Misteli laboratory), heterochromatin protein HP1α (purchased from addgene plasmid #17652, originally from Tom Misteli laboratory) and core histone H2B proteins following transient transfections. Transfections were done using Jetprime transfection reagent (Polyplus Transfection™). Experiments were performed on cells in an incubation stage heated to 37°C and supplied with 5% CO₂. For actin perturbation using drugs, FCS and FRAP data were collected 40 min after the drugs were applied; for immunofluorescence imaging, the cell were

fixed 1-2 hrs after the drugs were applied. For cell culturing with serum starvation, the cells were trypsinized and seeded on glass surface dishes in 10% FBS DMEM medium and cultured for at least 3 hours. One set of dishes was allowed to grow in 10% FBS medium, and medium in another set of dishes was removed and washed 2 times with 1X PBS. Then DMEM without FBS was added and to let the cell grow for at least 24-48 hours.

Fluorescence Correlation Spectroscopy

The FCS data was collected using the Confocal Zeiss LSM 710 ConfoCor3 equipped with a water immersion objective (C-Apochromat, 40X, NA 1.2), and with the PMT detector for sensitive FCS signal detection. The calibration for maximum FCS signal was done by monitoring the signal intensity of atto 488 dye (Sigma-Aldrich®) at 5 nM concentration temperature controlled chamber at 25°C or at 37°C with 5% CO₂. This dye was also used for the monitoring of laser power. For the experiments involving cells, we used only eGFP-tag for all proteins, and probed with 488 nm laser, pinhole size of 37 μm, and 0.20 % of 65 mW Argon laser. The length of time for each measurement is 3 sec with at least 60 repetitions taken for each data point that was collected from a spot in the cell nucleus. For lamin A, the data was collected at the nuclear lamina layer. For HP1α, measurements were taken at two different loci near the nuclear lamina and in the nucleoplasm. To achieve this, the FCS focal point was brought slowly into the nucleus, e.g. in the case of lamin A, we observed a significant increase in the FCS signal of the protein. To obtain the data of either HP1α or H2B, the FCS focal point was moved further into the nucleus using the controller. All experiments involving live cells were done in the temperature controlled chamber at 37°C with 5% CO₂. Each FCS data presented in this study is consisted of at least 40 data sets. Each data set was analyzed separately with the Zen software that came with the microscope (Carl Zeiss GmbH), and a three-dimensional (3D) diffusion model fitted with a triplet state and two diffusion components was applied to fit the autocorrelation curve (see SI for more

information about the mathematical equations, fitting and calculations). A Table to show results of fitting using different fitting models is also presented in Table S1.

Fluorescence Recovery after Photobleaching

Fluorescence recovery was monitored on bleach spots through confocal slices passing through central planes (of H2B and lamin A) and through basal-apical planes (of HP1 α) transfected nuclei. Imaging was done on a Nikon A1R microscope using 100x/1.4 NA oil immersion objective, with a $\sim 1\mu\text{m}$ spot photobleached and monitored to obtain bleach recovery dynamics using custom routines written in MATLAB (MathWorks, USA). In the case of axial nuclear mobility, bleach spots were manually tracked prior to bleach recovery assessment.

Confocal imaging and analysis

Immunofluorescence images (512 x 512, 12 bit images with optimal pin hole sizes) were captured on a Nikon A1R microscope, using a 100x/1.4 NA oil immersion objective. Z-stacks of nuclei with step size of 0.4 - 0.8 μm were acquired. Quantitative assessment of protein intensity levels were done using custom routines written in MATLAB (MathWorks, USA) and plotted using OriginPro (OriginLab Corporation, 8.6.0). Total protein levels were quantified from summation of immunofluorescence intensity levels across basal to apical z-sections of nuclei from a population of cells for each of the different patterns and actin polymerization states. The ratio of total DNA heterochromatin to total euchromatin intensity, summed across basal-apical z-sections for each nucleus in the population of cells was computed to quantify the DNA heterochromatin/euchromatin ratio. The lamin A shape was defined as $4\pi A/P^2$, where A is the area, and P is the perimeter of the nuclear lamina. The variation in the shape of the lamina was quantified by heterogeneity in lamin shape measured from basal to apical sections across the height of the nucleus for cells of varying geometry.

The 3D rendering of the nucleus and heterochromatin foci structural organization was done using Imaris 7.6.1 (Bitplane). Confocal scanning z-sections were rendered to obtain heterochromatin foci surface area.

References

1. P. Isermann and J. Lammerding, *Current biology : CB*, 2013, 23, R1113-1121.
2. G. V. Shivashankar, *Annual review of biophysics*, 2011, 40, 361-378.
3. N. Wang, J. D. Tytell and D. E. Ingber, *Nature reviews. Molecular cell biology*, 2009, 10, 75-82.
4. G. Cavalli and T. Misteli, *Nature structural & molecular biology*, 2013, 20, 290-299.
5. T. Cremer and C. Cremer, *Nature reviews. Genetics*, 2001, 2, 292-301.
6. C. Lanctot, T. Cheutin, M. Cremer, G. Cavalli and T. Cremer, *Nature reviews. Genetics*, 2007, 8, 104-115.
7. E. Meshorer, D. Yellajoshula, E. George, P. J. Scambler, D. T. Brown and T. Misteli, *Developmental cell*, 2006, 10, 105-116.
8. T. Misteli, *Science*, 2001, 291, 843-847.
9. R. D. Phair, P. Scaffidi, C. Elbi, J. Vecerova, A. Dey, K. Ozato, D. T. Brown, G. Hager, M. Bustin and T. Misteli, *Molecular and cellular biology*, 2004, 24, 6393-6402.
10. E. C. Tapley and D. A. Starr, *Current opinion in cell biology*, 2013, 25, 57-62.
11. H. Taniura, C. Glass and L. Gerace, *The Journal of cell biology*, 1995, 131, 33-44.
12. D. K. Shumaker, E. R. Kuczmarski and R. D. Goldman, *Current opinion in cell biology*, 2003, 15, 358-366.
13. A. Mattout, M. Goldberg, Y. Tzur, A. Margalit and Y. Gruenbaum, *Journal of cell science*, 2007, 120, 77-85.
14. D. N. Simon, M. S. Zastrow and K. L. Wilson, *Nucleus*, 2010, 1, 264-272.
15. J. Lammerding, P. C. Schulze, T. Takahashi, S. Kozlov, T. Sullivan, R. D. Kamm, C. L. Stewart and R. T. Lee, *The Journal of clinical investigation*, 2004, 113, 370-378.
16. C. Y. Ho, D. E. Jaalouk, M. K. Vartiainen and J. Lammerding, *Nature*, 2013, DOI: 10.1038/nature12105.
17. J. M. Gonzalez-Granado, C. Silvestre-Roig, V. Rocha-Perugini, L. Trigueros-Motos, D. Cibrian, G. Morlino, M. Blanco-Berrocal, F. G. Osorio, J. M. Freije, C. Lopez-Otin, F. Sanchez-Madrid and V. Andres, *Science signaling*, 2014, 7, ra37.
18. J. S. Lee, C. M. Hale, P. Panorchan, S. B. Khatau, J. P. George, Y. Tseng, C. L. Stewart, D. Hodzic and D. Wirtz, *Biophysical journal*, 2007, 93, 2542-2552.
19. S. B. Khatau, C. M. Hale, P. J. Stewart-Hutchinson, M. S. Patel, C. L. Stewart, P. C. Searson, D. Hodzic and D. Wirtz, *Proc Natl Acad Sci U S A*, 2009, 106, 19017-19022.
20. N. M. Ramdas and G. V. Shivashankar, *Journal of molecular biology*, 2015, 427, 695-706.
21. Q. Li, A. Kumar, E. Makhija and G. V. Shivashankar, *Biomaterials*, 2014, 35, 961-969.
22. N. Jain, K. V. Iyer, A. Kumar and G. V. Shivashankar, *Proc Natl Acad Sci U S A*, 2013, 110, 11349-11354.
23. G. Gerlitz and M. Bustin, *Journal of cell science*, 2010, 123, 2207-2217.
24. K. V. Iyer, S. Pulford, A. Mogilner and G. V. Shivashankar, *Biophysical journal*, 2012, 103, 1416-1428.
25. M. Versaevel, T. Grevesse and S. Gabriele, *Nature communications*, 2012, 3, 671.

26. G. Gerlitz, O. Reiner and M. Bustin, *Cellular and molecular life sciences : CMLS*, 2013, 70, 1255-1268.
27. T. Misteli, *Cell*, 2007, 128, 787-800.
28. E. I. Campos and D. Reinberg, *Annual review of genetics*, 2009, 43, 559-599.
29. B. D. Strahl and C. D. Allis, *Nature*, 2000, 403, 41-45.
30. T. Cheutin, A. J. McNairn, T. Jenuwein, D. M. Gilbert, P. B. Singh and T. Misteli, *Science*, 2003, 299, 721-725.
31. S. A. Jacobs and S. Khorasanizadeh, *Science*, 2002, 295, 2080-2083.
32. N. Dillon, *Developmental cell*, 2008, 15, 182-186.
33. P. Fraser and W. Bickmore, *Nature*, 2007, 447, 413-417.
34. B. Kalverda, M. D. Roling and M. Fornerod, *FEBS letters*, 2008, 582, 2017-2022.
35. A. Buxboim, J. Swift, J. Irianto, K. R. Spinler, P. C. Dingal, A. Athirasala, Y. R. Kao, S. Cho, T. Harada, J. W. Shin and D. E. Discher, *Current biology : CB*, 2014, 24, 1909-1917.
36. I. M. Nooren and J. M. Thornton, *The EMBO journal*, 2003, 22, 3486-3492.
37. S. E. Ozbabacan, H. B. Engin, A. Gursoy and O. Keskin, *Protein engineering, design & selection : PEDS*, 2011, 24, 635-648.
38. T. Shimi, K. Pflieger, S. Kojima, C. G. Pack, I. Solovei, A. E. Goldman, S. A. Adam, D. K. Shumaker, M. Kinjo, T. Cremer and R. D. Goldman, *Genes & development*, 2008, 22, 3409-3421.
39. M. R. Bubb, A. M. Senderowicz, E. A. Sausville, K. L. Duncan and E. D. Korn, *The Journal of biological chemistry*, 1994, 269, 14869-14871.
40. M. Coue, S. L. Brenner, I. Spector and E. D. Korn, *FEBS letters*, 1987, 213, 316-318.
41. Y. Wang, S. Maharana, M. D. Wang and G. V. Shivashankar, *Scientific reports*, 2014, 4, 4477.
42. G. C. Moser, R. J. Fallon and H. K. Meiss, *Journal of cellular physiology*, 1981, 106, 293-301.
43. R. D. Moir, M. Yoon, S. Khuon and R. D. Goldman, *The Journal of cell biology*, 2000, 151, 1155-1168.
44. S. Gilchrist, N. Gilbert, P. Perry, C. Ostlund, H. J. Worman and W. A. Bickmore, *BMC cell biology*, 2004, 5, 46.
45. G. Galiova, E. Bartova, I. Raska, J. Krejci and S. Kozubek, *European journal of cell biology*, 2008, 87, 291-303.
46. S. Melcer, H. Hezroni, E. Rand, M. Nissim-Rafinia, A. Skoultchi, C. L. Stewart, M. Bustin and E. Meshorer, *Nature communications*, 2012, 3, 910.
47. H. Kimura and P. R. Cook, *The Journal of cell biology*, 2001, 153, 1341-1353.
48. D. Bhattacharya, A. Mazumder, S. A. Miriam and G. V. Shivashankar, *Biophysical journal*, 2006, 91, 2326-2336.
49. K. P. Muller, F. Erdel, M. Caudron-Herger, C. Marth, B. D. Fodor, M. Richter, M. Scaranaro, J. Beaudouin, M. Wachsmuth and K. Rippe, *Biophysical journal*, 2009, 97, 2876-2885.
50. R. Festenstein and L. Aragon, *Genome biology*, 2003, 4, 342.
51. A. J. Bannister, P. Zegerman, J. F. Partridge, E. A. Miska, J. O. Thomas, R. C. Allshire and T. Kouzarides, *Nature*, 2001, 410, 120-124.
52. M. Lachner, D. O'Carroll, S. Rea, K. Mechtler and T. Jenuwein, *Nature*, 2001, 410, 116-120.

Figure Legends

Figure 1. Cell geometric constraints modulate the structural organization of nuclear lamin A/C protein. **(A)** Representative confocal images of phalloidin-stained actin and Hoechst 33342 stained DNA along with immunostained lamin A/C in NIH3T3 fibroblasts. Cells were cultured on different geometric patterns: rectangular $1800 \mu\text{m}^2$ patterns and circular $500 \mu\text{m}^2$ patterns in contrast to cells grown on un-patterned geometry (n=15-20). **(B)** The changes in lamin A/C architecture in response to substrate geometry are demonstrated by the box plot of alterations in global lamin A/C levels with cellular geometry ($p < 0.001$). Scale bar = $5 \mu\text{m}$.

Figure 2. Geometric constraints reveal differential modulation of nuclear protein diffusion timescales using FCS. **(A-B)** Diffusion characteristics of nuclear proteins examined by autocorrelations curves for the FCS data fitted using a two-component 3D diffusion model. Distribution profiles **(A)** is the diffusion time fitted from all FCS experiments in our study, and **(B)** is the transient interaction time distribution from FCS experiments on cell- (Unpatterned). Investigation of the nuclear proteins: lamin A (top row), HP1 α (middle row), and H2B (bottom row) reveal their diffusion characteristics for cells seeded on un-patterned surfaces (black color). **(C-E)** Modulation of distribution profiles of interaction timescales for the nuclear proteins due to cellular geometry. Cells have different diffusion characteristics depending on their seeding on $1800 \mu\text{m}^2$ rectangular patterns (upper row; grey color), or on $500 \mu\text{m}^2$ circular patterns (lower row; red color).

Figure 3. Pharmacological perturbation of actin organization results in nuclear protein interaction timescales which mirror the timescales from geometric constraints. **(A)** Basal and apical confocal images of phalloidin-stained actin and Hoechst-stained DNA of nuclei in cells treated with drugs that alter the actin polymerization state. **(B-D)** Distribution profiles of interaction timescales obtained by fitting of two-component anomalous diffusion for nuclear

proteins: (B) Lamin A, (C) HP1 α and (D) H2B, in cells with perturbed actin architecture. Mean interaction timescales and distribution profiles are shown for cells either without drug treatment (NoDrugs; top row, black color), or incubated under the influence of actin stabilizing drug Jas (middle row, gray color), or actin depolymerizing drug LatA (bottom row, red color). Scale bar = 5 μ m.

Figure 4. Mobility of nuclear proteins is differentially modulated by cellular geometric constraints. FRAP study of eGFP-tagged nuclear proteins reveals differential recovery kinetics due to altered actin architecture. **(A, D, G)** A time-lapse series of confocal images illustrate fluorescence recovery following bleach of the nuclear proteins: (A) Lamin A, (D) HP1 α , and (G) H2B. The fluorescence recovery kinetics for Lamin A (B–C), HP1 α (E–F) and H2B (H–I) for cells with actin organization constrained via geometry or perturbed via drugs. **(B, E, H)** Differential modulation in the mobility of nuclear proteins due to rectangular and circular cellular geometry in contrast to un-patterned geometry. **(C, F, I)** Alteration in nuclear protein kinetics due to actin stabilization drug (Jas) and actin depolymerization (LatA) drugs in contrast to no treatment (NoDrugs). Inset shows changes in mobile fraction and recovery timescale of nuclear proteins as a result of changes in actin architecture due to altered cellular geometry and actin polymerization state. n=15-20. Scale bar = 5 μ m. Error bars indicate mean \pm SE; **p < 0.001.

Figure 5. Perinuclear actin architecture differentially controls chromatin spatial organization. **(A)** Representative confocal images of Hoechst stained DNA organization along with immunostained heterochromatin protein HP1 α and stained nuclear epigenetic marker H3K9me3 on different cellular geometries. **(B-C)** Box plots of the global protein intensities as obtained from immunofluorescence studies of (B) H3K9me3 and (C) HP1 α un-patterned cells (black color) in contrast to cells constrained by rectangular (gray color) or circular

geometry (red color), n=15-20. **(D)** Quantitative assessment of changes in heterochromatin foci altered due to cellular geometry ($p < 0.005$). Scale bar = 5 μm .

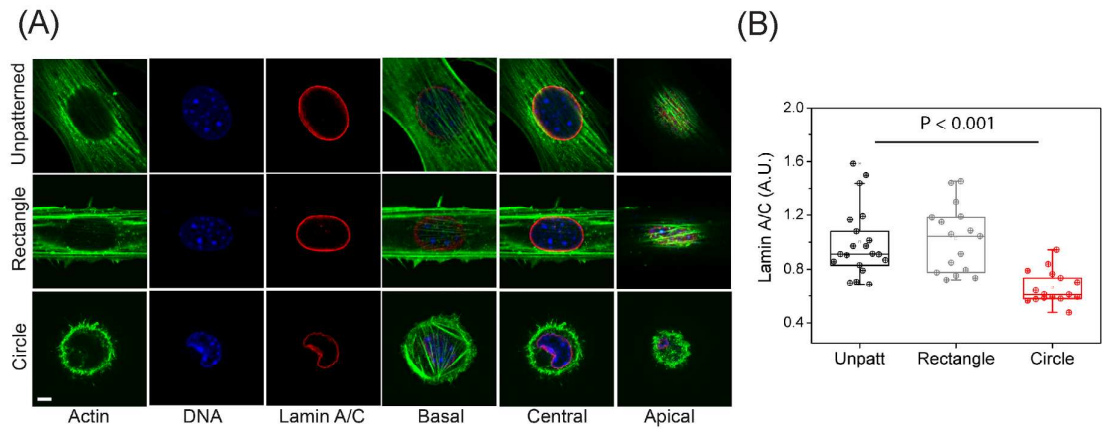


Figure 1.

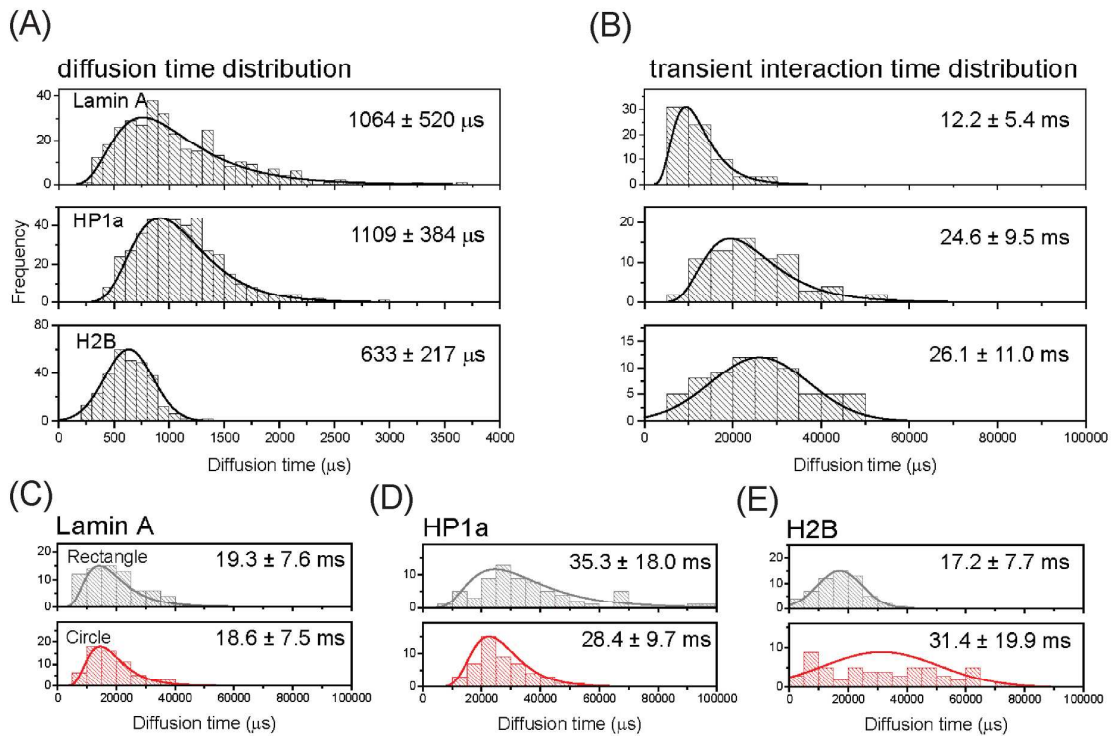


Figure 2.

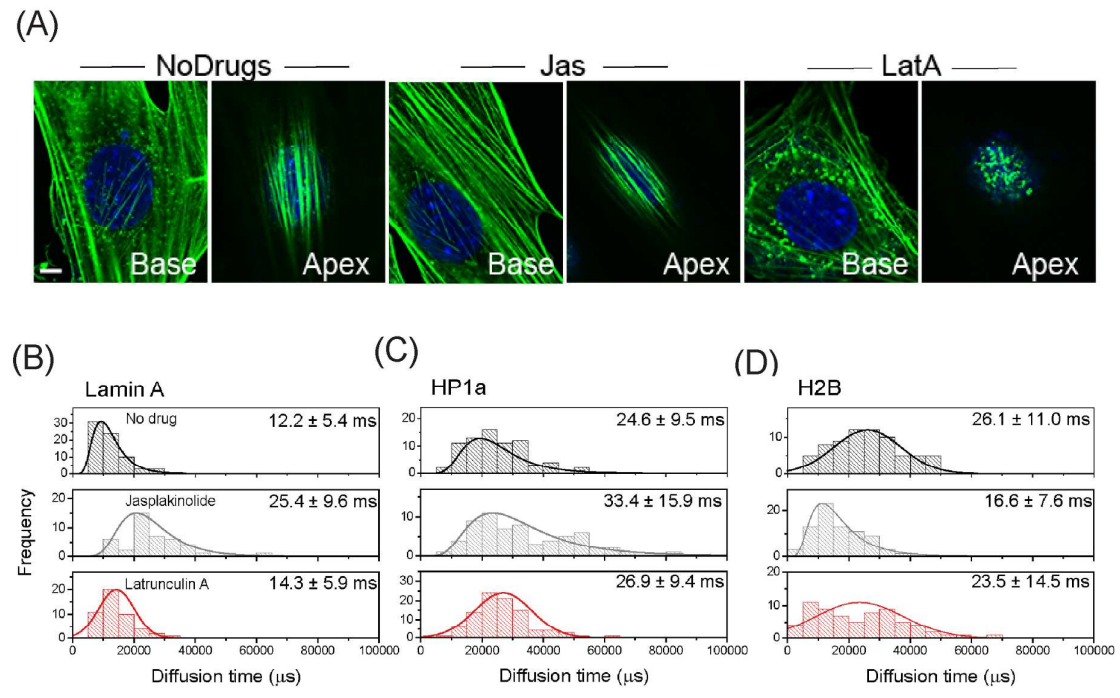


Figure 3.

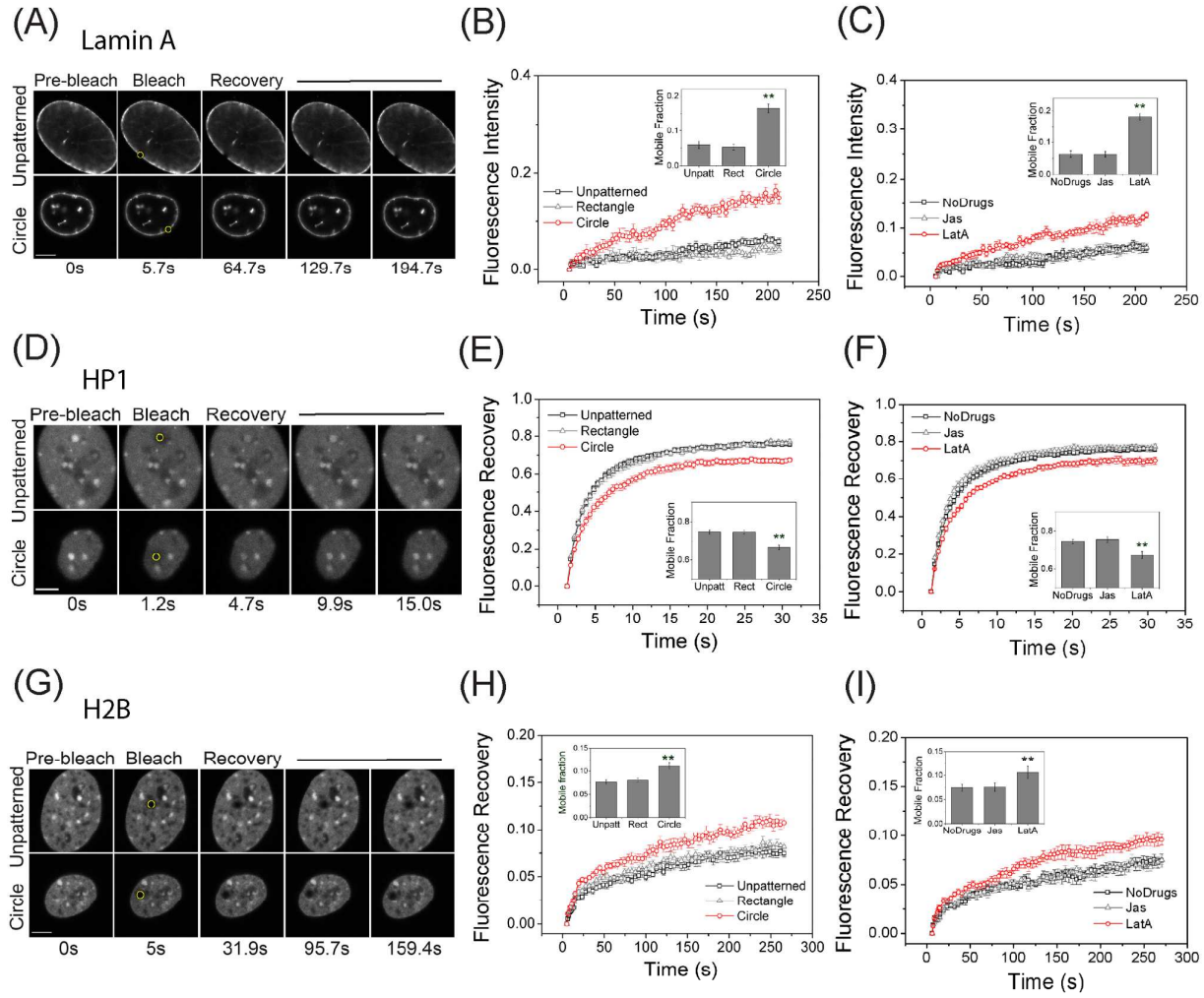


Figure 4.

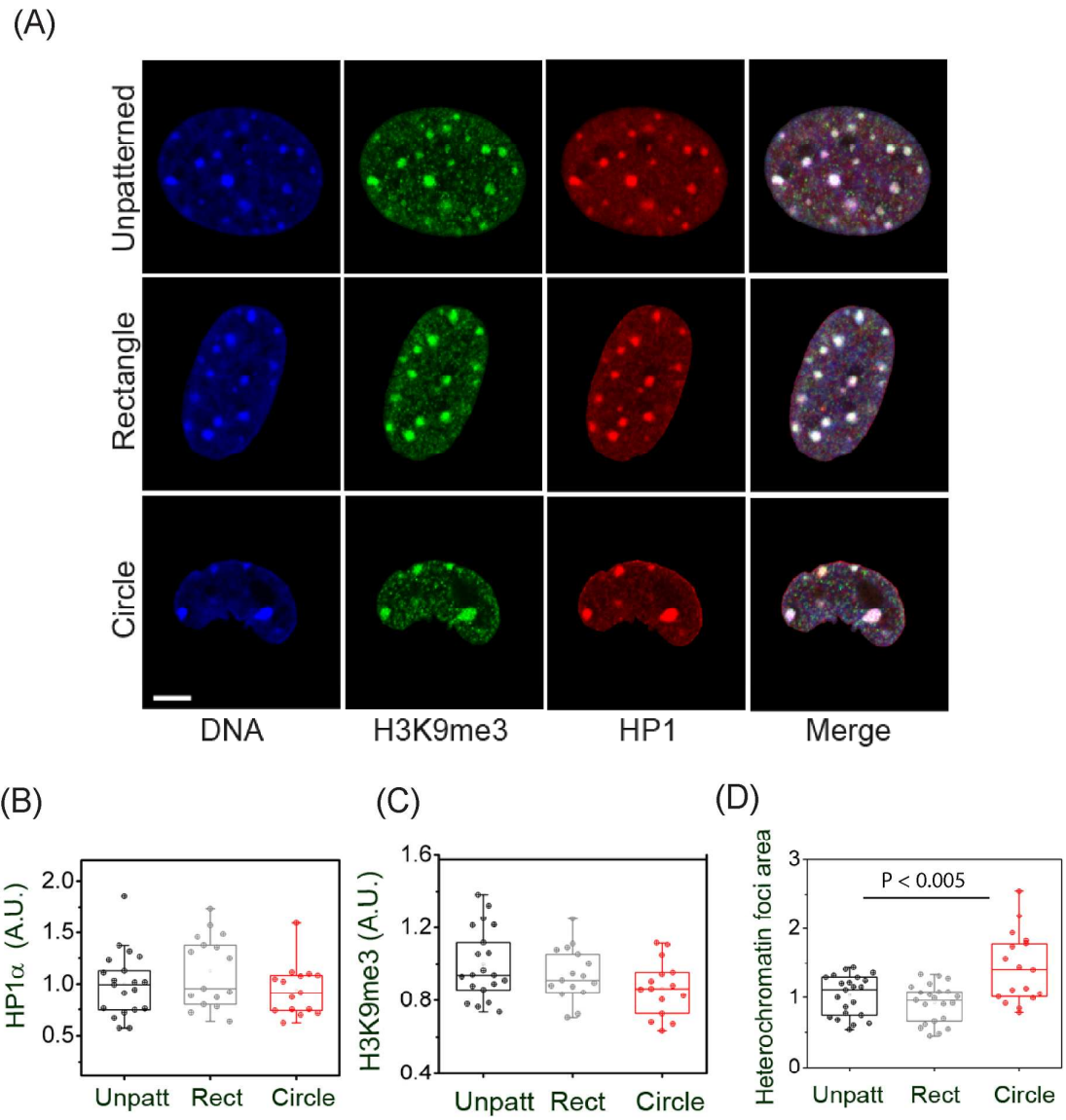


Figure 5.

TEXTUAL ABSTRACT

Cellular mechanical signals via the actin cytoskeleton regulate DNA packing by altering the dynamics of nuclear structure proteins.

GRAPHICAL ABSTRACT**Lamin A, HP1 α , Histone H2B protein dynamics**